Available online at www.sciencedirect.com
ScienceDirect
Comput. Methods Appl. Mech. Engrg. 367 (2020) 113096
Computer methods in applied mechanics and engineering
www.elsevier.com/locate/cma

Transient sensitivity analysis and topology optimization for particle motion in steady state laminar fluid

Gil Ho Yoon

School of Mechanical Engineering, Hanyang University, Seoul, South Korea

Received 19 November 2019; received in revised form 4 March 2020; accepted 23 April 2020
Available online 15 May 2020

Abstract

A new topology optimization scheme considering the transient particle motion in steady state laminar fluid is developed in the present study. To efficiently control the transient motion of particles in steady state laminar fluid, it is possible to apply the fluid topology optimization method considering the particle and fluid interaction condition. Inside steady state laminar fluid, particles move due to the fluid drag forces which are the functions of the fluid velocity and the velocities of particles. Indeed, the motions of particles can be controlled and optimized by changing the movement of fluid for several engineering applications. From a topology optimization point of view, the design variables determining the Darcy's forces in fluid are optimized in order to control the velocities of particles. The transient sensitivity analysis is newly derived considering the steady laminar fluid and Newton's 2nd equation. Through several optimization examples, the validity and the application of the present topology optimization method are illustrated.

Keywords: Topology optimization; Particle–fluid interaction; Transient adjoint sensitivity analysis; Transient analysis; Drag force

1. Introduction

This research develops a new topology optimization scheme to optimize the motion of particle in steady state laminar flow. It is one of the important engineering subjects to control the motions of particles suspended in a carrier fluid for air purifier, air cleaner, or cell separation device in bio engineering. Continuous manipulation and separation of micro particles for a wide range of engineering applications in micro-manufacturing, biology, medicine and etc have been important [1–8]. One of the common techniques of particle manipulation is to use the viscosity force of laminar flow. Indeed microfluidic systems have been developed and have been very useful tools for particle handling. For active manipulation, it is also viable to apply externally applied force. To control this particle motion in laminar flow without external force, the streamline or the channel shape can be optimized. To our best knowledge, there have been no research to topologically optimize fluid structure or channel to manipulate the motion of particle. Thus, the aim of this study is to develop the transient sensitivity analysis of the particle motion and the new topology optimization scheme formulations for particle motion in steady state laminar flow as shown in Fig. 1.

To our best knowledge, there is few research considering the motion of particle in fluid in topology optimization. After the introduction of the concept of topology optimization, many creative structural optimization methods

E-mail addresses: ghy@hanyang.ac.kr, gilho.yoon@gmail.com.

https://doi.org/10.1016/j.cma.2020.113096
0045-7825/

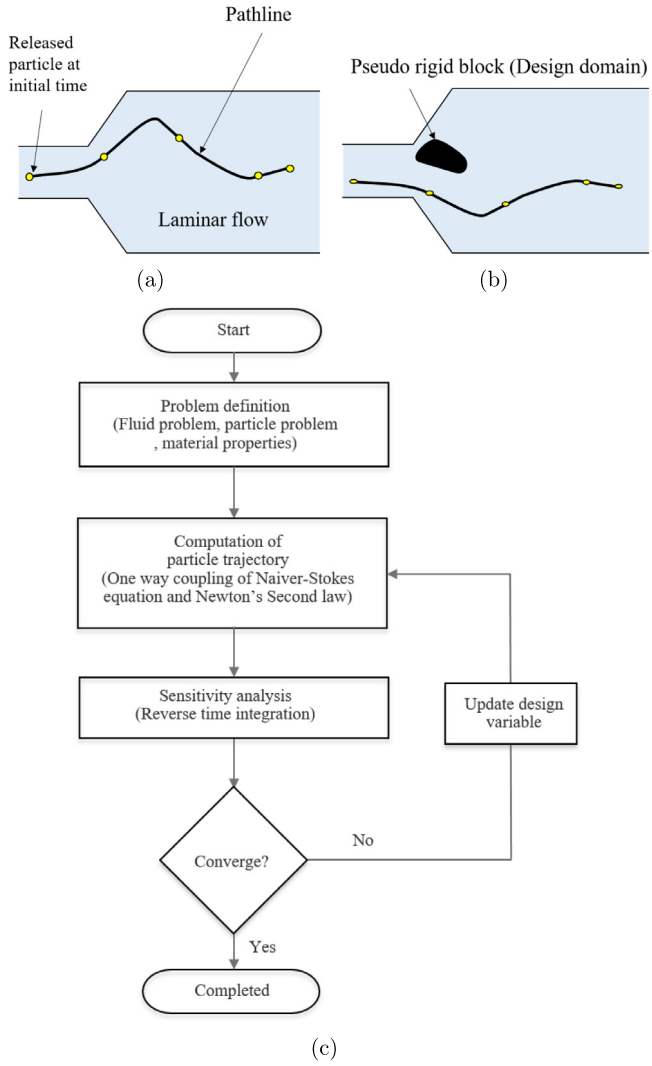

Fig. 1. Multiphysics analysis and topology optimization of particle in laminar flow.

such as the density based topology optimization with the SIMP (Solid Isotropic Material with Penalization) penalization, the level-set approach, the Moving Morphable Component, and other approaches have been developed and applied [9–12]. Not requiring a prior given optimal topology, the topology optimization scheme can provide optimal layouts for many engineering structures, and has been widely applied [11,13–19]. Among many interesting subjects related with topology optimization, the topology optimization for fluid domain has been an important subject. In [13], the topology optimization of fluid domain with the kinetic model is solved. In [14], the adjoint sensitivity analysis for turbulent problem was derived and the topology optimization for turbulent flow was researched in [20]. In [19], the sensitivity analysis and topology optimization for unsteady flow problem are formulated and presented. The conjugate heat transfer problems are considered by topology optimization in [16,21]. In [18], the lattice Boltzmann method was introduced for the conjugate heat transfer problem. See [22] for the detailed review for topology optimization for the conjugate heat transfer problem. The design variables assigned to each cell or the finite elements interpolate the material properties of the physical equations of interest. The most straightforward interpolation scheme may be the SIMP scheme [9]. The present study tries to contribute a topology optimization with the SIMP scheme considering the microparticle motion in fluid [23–25].

The particle manipulation has been one of the important subject in various engineering fields, i.e., microfluidics system, micro-manufacturing, biology, and medicine. In these applications, the overall effect of particles on flow dynamics is one of the important aspects (See [7] for an overview of the computation methods of the fluid–particle interaction). Common approach to manipulate the motions of particles mainly replies on laminar flow or external forces such as electrostatic, electromagnetic forces, and micro-scale hydrodynamic effects [26,27]. As it is possible to control and increase the sensitivity, microfluidic systems become promising to manipulate small particles. Furthermore it is also possible to control drag forces on particles by changing the outlines of particles. For the computation of the motion of the large particle affecting fluid motion, the direct simulation of particle–fluid motion has been conducted [3–5,7]. It shows the promising applications for the lubrication transport of solid particles and particle clustering in fluid. Research in different fields of computational science and engineering has resulted in well-established approaches to simulate the interaction. To our best knowledge, however, the topology optimization with the coupled consideration of particle and fluid together is not trivial as it requires the interplay of various assumptions, algorithms and the sensitivity analysis. To simulate the interaction phenomena between solid particles and liquid, the transient or steady-state Navier–Stokes equation for fluid and Newton's equations for transient motion for particle should be solved. Depending on the sizes of particles of interest, different simulation approaches can be employed. In the presence of finite size particles, the particle inertia (rotation) is non-negligible and the carried fluid becomes not dilute. In order to simplify the analysis condition, this research assumes that small particle does not contribute the motion of steady-state laminar fluid, i.e. one way coupling from fluid to particle. The one-way coupled multiphysics equations can provide us all the details of the flow and the interaction with small particles. Then the transient motion of the particle can be computed and the clear understandings of the particle motion can be possible. Based on these understandings, many innovative researches have been conducted.

Based on the one-way coupling multiphysics analysis, the present study develops a new topology optimization scheme to control the motion of particle. To control the motion of particle, several heuristic approaches and the size optimization have been proposed (See [23,24] and references therein). The fluid motion becoming complex, the difficulties arise to use simple channel geometries. Indeed it is common to rely on Computational Fluid Dynamic (CFD) simulation to determine optimal profiles of channels. To numerically simulate the motion of particle in flow, the two governing equations, i.e., Navier–Stokes equation and Newton's 2nd law, can be coupled and analyzed. Due to the movement of fluid, the drag force is exerted on particles and it is possible to control the fluid velocities in order to have the target motion of particle. Apart from the current challenges for these simulations, it is also difficult to obtain the sensitivity analysis for structural optimization. Depending on the simulation conditions and the objective function, the sensitivity analysis should be newly derived. The present study assumes the steady state fluid and neglects the influence of particle on fluid. The contact of particle towards wall and another particle is also neglected. In the Navier–Stokes equation, the Darcy's force is added to model the fluid in porous media and parameterized with respect to the spatial design variables (the constant design variables at each finite elements). With the above assumptions and the simplifications, the transient sensitivity analysis can be derived in the present study. To our best knowledge, this subject has not been researched yet from the topology optimization point of view. After presenting the modification of the multiphysics problem and the transient sensitivity analysis, it is possible to find out the optimal distributions of porous media (pseudo rigid wall) to control the motion of the particle as shown in Fig. 1.

The paper is organized as follows. Section 2 provides some backgrounds to the coupled analysis for particle and steady-state fluid motion and newly develops the sensitivity analysis of the objective function with particle motion. In Section 3, several topology optimization formulations and studies are considered. Section 4 provides the conclusions and suggestions for future research topics.

2. Transient sensitivity analysis for particle motion in fluid

This section delivers the theories and assumptions of the multiphysics analysis of fluid and particle and develops a new topology optimization procedure. The simulation of the particle motion in laminar flow requires the multiphysics analysis of Navier–Stokes equation and Newton's second law. To simulate the motion of particle, the segregation approach for the multiphysics analysis is employed. To conduct the topology optimization considering the motion of particle, the material interpolation of the involved material properties needs to be formulated to model fluid as well as porous material (pseudo rigid body) followed by the detailed topology optimization procedure and the transient sensitivity analysis.

2.1. Governing equation: Navier–Stokes equation and Newton's equation

An overwhelming amount of literature are available for microfluid analysis with micro particles (see [18,23–25,28] and references therein). The analysis of suspension mechanics of particle needs the hydrodynamic interactions between particles suspended in viscous fluid. With sufficient small particles, the effect of the particles for fluid motion can be neglected [18,23–25,27]. The motions of large particles affect the fluid motion and it is also one of the important subjects in the study of particles in fluid. The present study limits our consideration to the movement of small particles inside laminar flow.

To analyze the laminar fluid motion with the Darcy's force, $\alpha\mathbf{u}$, the Navier–Stokes equation for fluid domain can be modified as follows:

$$\begin{aligned} &\rho(\mathbf{u}\cdot\nabla)\mathbf{u} = \nabla\cdot\left[-p\mathbf{I}+\mu(\nabla\mathbf{u}+\nabla\mathbf{u}^{\mathrm{T}})\right]-\alpha\mathbf{u} \quad \text{on} \quad \Omega \\ &\nabla\cdot(\rho\mathbf{u}) = 0 \end{aligned} \tag{1}$$

with the following boundary conditions,

$$\begin{aligned} &\text{No-slip boundary condition: } \mathbf{u}=\mathbf{0} \quad \text{on} \quad \Gamma_{u0} \\ &\text{Inflow/outflow boundary condition: } \mathbf{u}=\mathbf{u}^{*} \quad \text{on} \quad \Gamma_{u*} \\ &\text{Pressure boundary condition: } \left[-p\mathbf{I}+\mu(\nabla\mathbf{u}+\nabla\mathbf{u}^{\mathrm{T}})\right]\cdot\mathbf{n} = p_p\mathbf{n} \quad \text{on} \quad \Gamma_{p}{}^{*} \end{aligned} \tag{2}$$

where the control volume is denoted by Ω. The fluid velocity, the fluid pressure, the mass density, and the dynamic viscosity are denoted by $\mathbf{u}$, p, ρ, and, μ, respectively. The no-slip boundary condition and the inflow/outflow boundary conditions of $\mathbf{u}^{*}$ are defined along Γ_{u0} and Γ_{u*}, respectively. The pressure boundary condition of p_p is defined along $\Gamma_{p}{}^{*}$. The normal direction vector is denoted by $\mathbf{n}$. The Darcy's force is defined as follows:

$$\alpha = \alpha_{max}\boldsymbol{\gamma}^{n} \tag{3}$$

Note that compared with the original Navier–Stokes equation, the Darcy force $\alpha\mathbf{u}$ is added for the fluid topology optimization with the maximum Darcy's force α_{max} and the force is interpolated as (3) with respect to the design variables $\boldsymbol{\gamma}$ with the SIMP penalization n between 3 and 5. The Darcy's force term can be interpolated to model the pseudo solid near zero velocities and the fluid domain. This approach allows the spatial distributions of material to find out an optimal layout in fluid problem [2,6,19,23,25]. For the analysis of the motion of small particle in fluid, the following Newton's 2nd law can be analyzed ignoring the rotational motions of particles; For the finite-size particles, not only the net force but also the net momentum with the momentum inertia of particles should be considered.

$$\frac{d}{dt}(m_p\mathbf{v}) = m_p F_D(\mathbf{u}-\mathbf{v}), \quad \frac{d\mathbf{X}}{dt} = \mathbf{v} \tag{4}$$

where the coefficient, F_D, is set as [29],

$$F_D = \frac{18\mu}{\rho_p d_p^2} \tag{5}$$

where the mass, diameter, density and velocity of particle are denoted by m_p, d_p, ρ_p and $\mathbf{v}$, respectively. The drag force inside the laminar fluid is formulated as the function of the difference of the velocities of the particle and the fluid , i.e., $m_p F_D(\mathbf{u}-\mathbf{v})$ that implies that the drag force acts opposite to the relative motion of any object moving with respect to fluid. Depending on the simulation conditions, it is possible to introduce the different formulation [27,29–31]. The absolute coordinate of the particle is denoted by $\mathbf{X}$ and without the loss of generality, the representative coefficient F_D can be simply formulated as Eq. (5) proposed at the technical report [29] for the particle motion behind a normal shock. For the applications of the cell separation in microfluidics, it is also possible to add more forces at the right side of Eq. (4). In the present study, we do not consider any other force except the drag force often called air resistance or fluid resistance acting opposite to the relative motion. Note that in addition to Eq. (4), the rotational motion of particle can be considered [27,30]. In order to simulate the trajectory of particle, the above two coupled equations can be solved with the staggered analysis in the framework of the finite element procedure shown in Fig. 1.

2.2. Transient sensitivity analysis of particle motion

As the present study limits the laminar flow and neglects the effect of the particle on fluid, it is possible to summarize the following aspects which are crucial in the formulation of the objective function and the transient sensitivity analysis.

1. The steady-state laminar Navier–Stokes equation is considered where Newton's 2nd law requires a transient analysis.
2. By neglecting the effect of the mass particle on fluid, a staggered analysis approach can be adopted, i.e., the Newton' 2nd law is solved after the solution of the laminar Navier–Stokes equation whose boundary flow is very smooth while the boundary flow of turbulent flow needs the consideration of swirls or eddies. This also simplifies the finite element simulation to take it to account the remeshing the fluid as the particle evolves.
3. Due to the transient analysis of the particle, the transient sensitivity analysis accompanied with the steady state fluid solver should be newly carried out; to our best knowledge, there is no precedent research regarding the sensitivity of the motion of particle considering the motion of fluid.
4. The motion of particle in fluid is only considered. In other words, the sensitivity analysis considering the nonlinear contact of the particle towards the pseudo rigid body modeled with the large Darcy's force has not been researched. Indeed, this research limits the simulation and the optimization conditions without the contact of the particle with the pseudo rigid body and the boundary conditions.
5. To simplify the optimization formulation, the contact among particles is also ignored; as the analysis of the contact among particles is itself a very challenging issue, this research does not consider the contact and this assumption simplifies the procedure as only one particle can be simulated. The simulation of multiple particles can be conducted independently.

To allow the topology optimization considering the motion of the particle due to the drag force, the material interpolation scheme should be developed properly. The design variables, $\boldsymbol{\gamma}$, are assigned to each fluid finite elements. In the present study, it is assumed that the objective function is formulated only with the velocities of particle. With the conventional segregated analysis approach using the different governing equations for fluid domain and particle, it is possible to solve the trajectories of particles. Then, the transient sensitivity analysis should be derived.

$$\text{Objective function: } \int_0^{t_f} c(\mathbf{v})dt \tag{6}$$

In order to derive the transient sensitivity analysis of the objective function in (6) considering the fluid motion, the following Lagrange function, L, is formulated with the two Lagrange multipliers, $\boldsymbol{\lambda}$ and $\boldsymbol{\psi}$.

$$\begin{aligned} &L = \int_0^{t_f} c(\mathbf{v})dt + \int_0^{t_f} \boldsymbol{\lambda}^{\mathrm{T}}(\mathbf{M}\dot{\mathbf{v}} - \mathbf{F}(\mathbf{v},\mathbf{u}))\mathrm{d}t + \int_0^{t_f} \boldsymbol{\psi}^{\mathrm{T}}\mathbf{R}(\mathbf{u},\boldsymbol{\gamma})\mathrm{d}t \\ &\text{with } \mathbf{F}(\mathbf{v},\mathbf{u}) = \mathbf{M}F_D(\mathbf{u}-\mathbf{v}) \end{aligned} \tag{7}$$

where the mass matrix and the force vector are denoted by $\mathbf{M}$ and $\mathbf{F}$, respectively. As the Newton's equation is a transient analysis, the second term of Eq. (7) is integrated over the time interval from the initial time (0) to the final time (t_f). Note that the third term which is the residual equation $\mathbf{R}$ for the stead state Navier–Stokes equation is also integrated from the time interval too. The derivative of the Lagrange function with respect to the design variable, γ_e, is summarized as (8).

$$\frac{\partial L}{\partial \gamma_e} = \frac{\partial}{\partial \gamma_e}\int_0^{t_f} c(\mathbf{v})dt + \frac{\partial}{\partial \gamma_e}\int_0^{t_f} \boldsymbol{\lambda}^{\mathrm{T}}(\mathbf{M}\dot{\mathbf{v}} - \mathbf{F}(\mathbf{v},\mathbf{u}))dt + \frac{\partial}{\partial \gamma_e}\int_0^{t_f} \boldsymbol{\psi}^{\mathrm{T}}\mathbf{R}(\mathbf{u},\boldsymbol{\gamma})dt \tag{8}$$

The derivative of the objective function with respect to the design variable, γ_e, is further expanded as follows:

$$\begin{aligned} \frac{\partial L}{\partial \gamma_e} = &\int_0^{t_f} \left(\frac{\partial c}{\partial \mathbf{v}}\frac{\partial \mathbf{v}}{\partial \gamma_e}\right)\mathrm{d}t + \\ &\int_0^{t_f} \boldsymbol{\lambda}^{\mathrm{T}}\left(\mathbf{M}\frac{\partial \dot{\mathbf{v}}}{\partial \gamma_e} - \frac{\partial \mathbf{F}}{\partial \mathbf{v}}\frac{\partial \mathbf{v}}{\partial \gamma_e} - \frac{\partial \mathbf{F}}{\partial \mathbf{u}}\frac{\partial \mathbf{u}}{\partial \gamma_e}\right)\mathrm{d}t + \\ &\int_0^{t_f} \boldsymbol{\psi}^{\mathrm{T}}\left(\frac{\partial \mathbf{R}}{\partial \mathbf{u}}\frac{\partial \mathbf{u}}{\partial \gamma_e} + \frac{\partial \mathbf{R}}{\partial \gamma_e}\right)\mathrm{d}t \end{aligned} \tag{9}$$

Due to the difficulties in the differentiation of the fluid velocity with respect to the design variables and the velocity of the particle with respect to the design variables, the adjoint design variable method should be adopted. The differentiation terms are defined over the time domain. Thus it is possible to add all the terms inside the time integration.

$$\frac{\partial L}{\partial \gamma_e} = \int_0^{t_f} \left(\begin{array}{l} \frac{\partial c}{\partial \mathbf{v}} \frac{\partial \mathbf{v}}{\partial \gamma_e} + \boldsymbol{\lambda}^{\mathrm{T}} \left(\mathbf{M} \frac{\partial \dot{\mathbf{v}}}{\partial \gamma_e} - \frac{\partial \mathbf{F}}{\partial \mathbf{v}} \frac{\partial \mathbf{v}}{\partial \gamma_e} - \frac{\partial \mathbf{F}}{\partial \mathbf{u}} \frac{\partial \mathbf{u}}{\partial \gamma_e} \right) \\ + \boldsymbol{\psi}^{\mathrm{T}} \left(\frac{\partial \mathbf{R}}{\partial \mathbf{u}} \frac{\partial \mathbf{u}}{\partial \gamma_e} + \frac{\partial R}{\partial \gamma_e} \right) \end{array} \right) \mathrm{dt} \tag{10}$$

For the adjoint system analysis, the time differentiation, $\mathbf{M} \frac{\partial \dot{\mathbf{v}}}{\partial \gamma_e}$, is further expanded as follows:

$$\int_0^{t_f} \boldsymbol{\lambda}^{\mathrm{T}} \mathbf{M} \frac{\partial \dot{\mathbf{v}}}{\partial \gamma_e} dt = - \int_0^{t_f} \frac{d\boldsymbol{\lambda}^{\mathrm{T}}}{dt} \mathbf{M} \frac{\partial \mathbf{v}}{\partial \gamma_e} dt + \left(\left(\boldsymbol{\lambda}^{\mathrm{T}} \mathbf{M} \frac{\partial \mathbf{v}}{\partial \gamma_e} \right) \Big|_0^{t_f} \right) \tag{11}$$

After inserting the above expansion into (10), the following equation can be obtained.

$$\begin{array}{l} \frac{\partial L}{\partial \gamma_e} \\ = \int_0^{t_f} \boldsymbol{\psi}^{\mathrm{T}} \left(\frac{\partial \mathbf{R}}{\partial \gamma_e} \right) dt + \int_0^{t_f} \left(\frac{\partial c}{\partial \mathbf{v}} - \boldsymbol{\lambda}^{\mathrm{T}} \frac{\partial \mathbf{F}}{\partial \mathbf{v}} - \frac{d\boldsymbol{\lambda}^{\mathrm{T}}}{dt} \mathbf{M} \right) \frac{\partial \mathbf{v}}{\partial \gamma_e} dt \\ + \int_0^{t_f} \left(-\boldsymbol{\lambda}^{\mathrm{T}} \frac{\partial \mathbf{F}}{\partial \mathbf{u}} + \boldsymbol{\psi}^{\mathrm{T}} \frac{\partial \mathbf{R}}{\partial \mathbf{u}} \right) \frac{\partial \mathbf{u}}{\partial \gamma_e} dt + \left(\left(\boldsymbol{\lambda}^{\mathrm{T}} \mathbf{M} \frac{\partial \mathbf{v}}{\partial \gamma_e} \right) \Big|_0^{t_f} \right) \end{array} \tag{12}$$

After separately gathering the terms involved for $\frac{\partial \mathbf{v}}{\partial \gamma_e}$ and $\frac{\partial \mathbf{u}}{\partial \gamma_e}$ and letting the involved factors zeros, the following transient sensitivity analysis with the adjoint sensitivity equations in (14) and (15) can be derived.

$$\frac{\partial L}{\partial \gamma_e} = \int_0^{t_f} \boldsymbol{\psi}^{\mathrm{T}} \frac{\partial \mathbf{R}}{\partial \gamma_e} \mathrm{dt} \tag{13}$$

$$\text{Adjoint system 1} : \frac{d\boldsymbol{\lambda}^{\mathrm{T}}}{dt} \mathbf{M} = \left(\frac{\partial c}{\partial \mathbf{v}} - \boldsymbol{\lambda}^{\mathrm{T}} \frac{\partial \mathbf{F}}{\partial \mathbf{v}} \right) \tag{14}$$

with $\dot{\lambda} = 0$ and $\lambda = 0$ at $t = t_f$(Reversal time integration scheme)

$$\text{Adjoint system 2} : \int_0^{t_f} \left(-\boldsymbol{\lambda}^{\mathrm{T}} \frac{\partial \mathbf{F}}{\partial \mathbf{u}} + \boldsymbol{\psi}^{\mathrm{T}} \frac{\partial \mathbf{R}}{\partial \mathbf{u}} \right) \frac{\partial \mathbf{u}}{\partial \gamma_e} \mathrm{dt} = \mathbf{0} \tag{15}$$

After solving the adjoint sensitivity equation in (14) for $\boldsymbol{\lambda}$, it can be plugged into the adjoint sensitivity equation in (15) for $\boldsymbol{\psi}$. Note that the term $\boldsymbol{\lambda}^{\mathrm{T}} \frac{\partial \mathbf{F}}{\partial \mathbf{v}}$ in (14) can be treated as either the time dependent external force term or the time dependent damping term; If this term is numerically analyzed as the damping term, a care should be made in the sign of the damping term with the reversed time. In either case, the Lagrange multiplier $\boldsymbol{\lambda}$ is the solution of the second order differential equation with the time dependent force term or the time dependent damping term. In other words, the same numerical integration schemes and parameter settings for the forward system in (4) can be employed for the adjoint sensitivity equation in (14). The conditions of $\dot{\boldsymbol{\lambda}} = \mathbf{0}$ and $\boldsymbol{\lambda} = \mathbf{0}$ at $t = t_f$ removes the last terms of the final sensitivity equation and the adjoint sensitivity equation in (14) can be reformulated with the reversal time integration scheme. The second adjoint sensitivity equation in (15) can be interpreted as a series of the linear equations with the time dependent force term, $\boldsymbol{\lambda}^{\mathrm{T}} \frac{\partial \mathbf{F}}{\partial \mathbf{u}}$, and the time independent stiffness matrix, $\frac{\partial \mathbf{R}}{\partial \mathbf{u}}$; the time independent stiffness matrix is attributed to the assumption of the steady state fluid. As the tangent stiffness of the Navier–Stokes equation is used, the same boundary condition is imposed except the non-homogeneous Dirichlet boundary condition which is replaced by the homogeneous Dirichlet boundary condition. If transient fluid condition is considered, as a matter of course, the stiffness matrix of the second adjoint system should be a time dependent term. By considering this aspect, the time varying terms with $\boldsymbol{\psi}$ in the sensitivity analysis equation and the second adjoint system equation can be reformulated as the independent terms. In order to solve the forward equation and the derived sensitivity equations, the Newmark integration scheme is implemented. The present study seamlessly develops an in-house code for the implementation of the above equations in Matlab environment as shown in Fig. 1. First of all, the fluid simulation with 9 nodes is conducted by the Newton–Raphson iteration after the problem definitions of fluid and particle. After that, the Newton's equation for the particle movement is solved using the Newmark's scheme (Beta = 1/6, Gamma = 1/3) considering the current particle position and its associated fluid

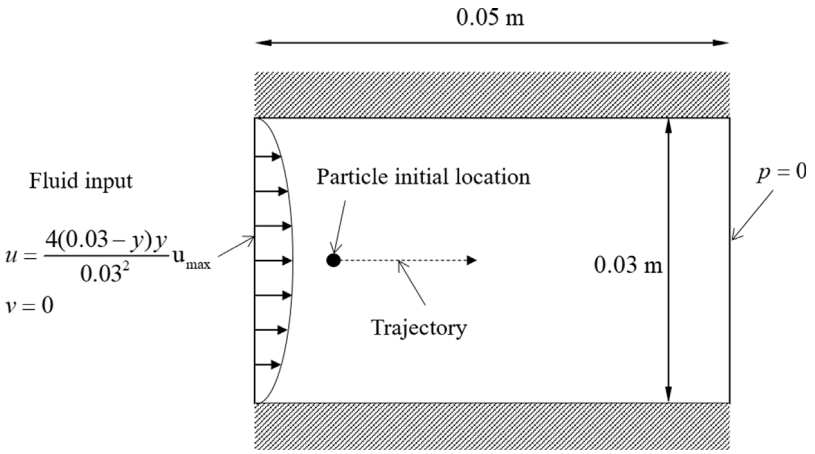

Fig. 2. Example 1. A channel design to maximize the square of the integration of the particle velocity (Input velocity: $u_{max} = 2.5 \times 10^{-3}$ m/s, Reynolds number: 213.0682 ($1000 \times 0.03 \times 2.5 \times 10^{-3}/352 \times 10^{-6}$, Fluid : density $= 1000$ kg/m^3, viscosity $= 352 \times 10^{-6}$ Pa×s, Particle: mass $= 1.0865 \times 10^{-13}$ kg, $F_D = 1.5857 \times 10^{-8} \frac{\mathrm{N{\cdot}s}}{\mathrm{kg{\cdot}m}}$), mass_0: 30 % of the design domain).

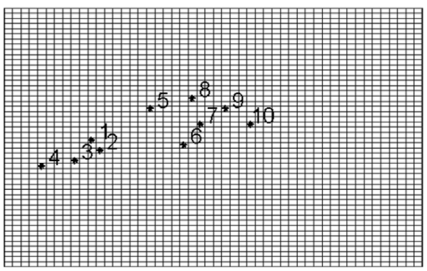

u_{max}: 0.0025 m/s^2, t_f=0.01 s, Δt=1×10^{-6}

	FDM	Sensitivity	Error (%)
1	-8.3774E-09	-8.3624E-09	0.1796
2	-6.1354E-09	-6.1244E-09	0.1794
3	-4.2549E-09	-4.2471E-09	0.1844
4	-3.1823E-09	-3.1765E-09	0.1821
5	-3.0063E-09	-3.0008E-09	0.1816
6	-2.4960E-09	-2.4915E-09	0.1808
7	-1.8845E-09	-1.8811E-09	0.1813
8	-1.7090E-09	-1.7059E-09	0.1813
9	-1.2188E-09	-1.2166E-09	0.1844
10	-1.0705E-09	-1.0685E-09	0.1836

u_{max}: 0.0025 m/s^2, t_f=5 s, Δt=2×10^{-6}

	FDM	Sensitivity	Error (%)
1	-1.9021E-06	-2.0135E-06	5.5353
2	-1.4541E-06	-1.5365E-06	5.3677
3	-2.0790E-06	-2.1979E-06	5.4087
4	-9.9811E-07	-1.0513E-06	5.0578
5	-9.0299E-07	-9.5133E-07	5.0805
6	-6.6128E-07	-6.9776E-07	5.2288
7	-5.4359E-07	-5.7290E-07	5.1151
8	-4.4981E-07	-4.7469E-07	5.2414
9	-5.6403E-07	-5.9153E-07	4.6480
10	-1.0373E-06	-1.0773E-06	3.7161

u_{max}: 0.25 m/s^2, t_f=0.01 s, Δt=1×10^{-6}

	FDM	Sensitivity	Error (%)
1	-1.3591E-06	-1.3568E-06	0.1666
2	-1.5763E-06	-1.5737E-06	0.1655
3	-1.0598E-06	-1.0580E-06	0.1692
4	2.9478E-08	2.9428E-08	0.1699
5	5.7968E-08	5.7871E-08	0.1675
6	-1.5602E-06	-1.5576E-06	0.1651
7	2.1694E-07	2.1659E-07	0.1652
8	-1.4049E-06	-1.4025E-06	0.1652
9	1.3717E-07	1.3694E-07	0.1644
10	-1.0259E-07	-1.0243E-07	0.1570

Fig. 3. Error comparison with the finite difference method (Diameter of particle: 4.78 μm, density of particle: 1900 kg/m^3, $F_D = \frac{18\mu}{\rho_p d_p^2} = 1.5857 \times 10^{-8} \frac{\mathrm{N{\cdot}s}}{\mathrm{kg{\cdot}m}}$).

velocity of (4). The first adjoint system is solved by the same Newmark's scheme with the time reversal scheme; as the same Newmark's scheme is employed, the velocity term should be multiplied by -1, i.e, the time reversal scheme. One of the problematic part in implementation lies in the computation of the particle velocity **u** considering the current particle position. In our simulation, the interpolation of the velocities of the fluid nodes is carried out by finding the natural coordinates inside the element containing the particle. A very small time step is used in the Newmark's scheme for the precise calculation and the numerical stability. Therefore, the computation of the natural

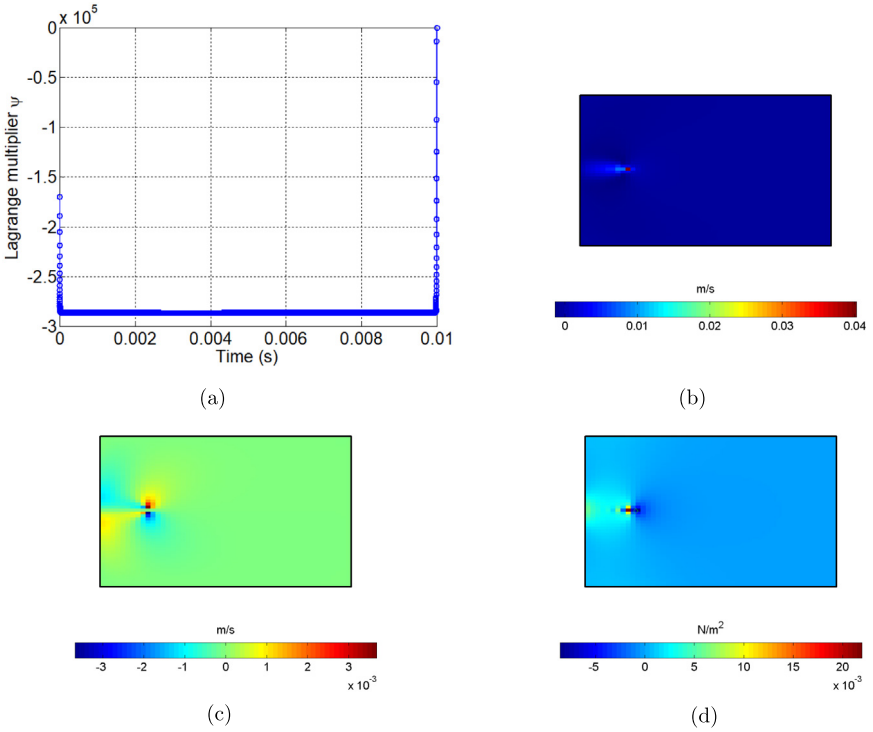

Fig. 4. Lagrange multipliers (Maximum velocity = 0.0025 m/s, initial design = 0.5, simulation time t_f: 0.01 s, time step = 10,000 steps (Newmark scheme)). (a) The x component of the Lagrange multiplier $\boldsymbol{\lambda}$, (b, c, and d) the x-velocity, the y-velocity and the pressure of $\int_0^{t_f}(\boldsymbol{\psi})\mathrm{dt}$.

coordinates can take a lot of time. By assuming the same finite elements of fluid, the efficient calculations of the natural coordinates were possible as follows:

$$\begin{aligned}\xi &= (x_{current} - \text{floor}(\tfrac{x_{current}}{\Delta x}) \times \Delta x) \times \tfrac{2}{\Delta x} - 1 \\ \eta &= (y_{current} - \text{floor}(\tfrac{y_{current}}{\Delta y}) \times \Delta y) \times \tfrac{2}{\Delta y} - 1\end{aligned} \tag{16}$$

where the natural coordinates are ξ and η and the current position of particle is denoted by $(x_{current}, y_{current})$. The element sizes in x and y directions are denoted by Δx and Δy, respectively. These natural coordinate values are also essential to define the derivative of the force with respect to the velocity, $\frac{\partial \mathbf{F}}{\partial \mathbf{u}}$, in the second adjoint system. For general shaped meshes, the interpolation of the fluid velocity is implemented. As the steady state fluid motion is assumed, the inversion of the tangent stiffness of the second adjoint system is carried out one time considering the time integration. Also the original design problem should be properly formulated with the sufficient penalization in order to make the design variables converged to 1 for rigid wall and 0 for fluid domain. As these discrete design variables are relaxed as the continuous variables, the intermediate design variables can appear. The areas with the intermediate design variables are interpreted as the porous areas with some moisture infiltration. In that case, extra penalization should be employed.

3. Numerical examples of topology optimization

To validate the concept of applying topology optimization to design fluid system for particle motion, this section solves several optimization problems. For the numerical examples, a silica particle with 4.78 μm for its diameter is assumed to be released and the dimensions of fluid domain are arbitrarily chosen. The simulation time and the time step are chosen observing the motion of the particle and the stability of the void design. Being no contact of the mass towards the wall and another particle, the consideration of only the motion of one particle is sufficient

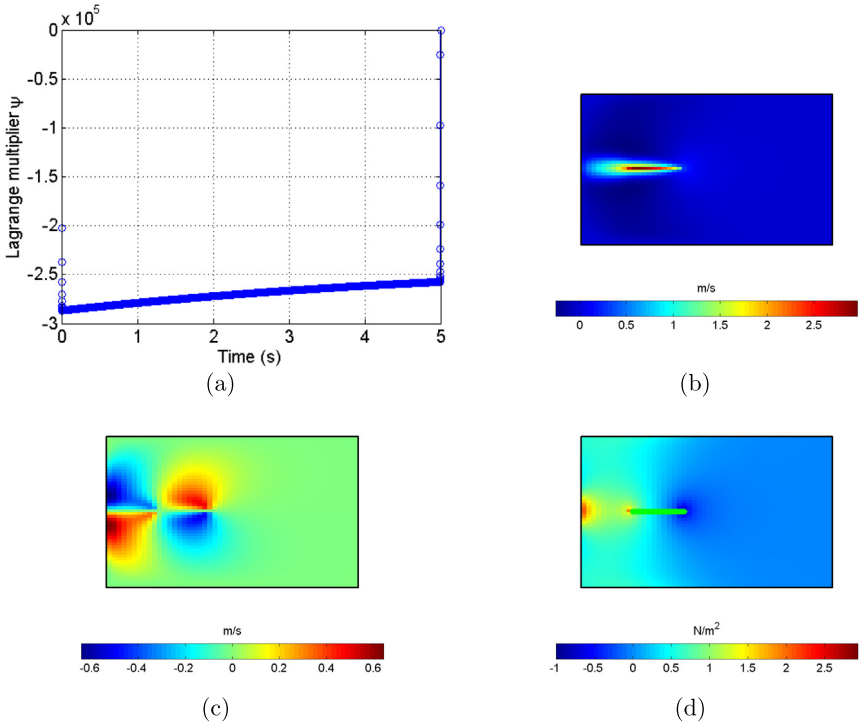

Fig. 5. Lagrange multipliers (Maximum velocity = 0.0025 m/s, initial design = 0.5, simulation time t_f: 5 s, time step = 2,500,000 steps (Newmark scheme)). (a) The x component of the Lagrange multiplier $\boldsymbol{\lambda}$, (b, c, and d) the x-velocity , the y-velocity and the pressure of $\int_0^{t_f} (\boldsymbol{\psi})\mathrm{dt}$.

to show the validity of the present approach. In order to solve the optimization problem, the method of moving asymptotes (MMA) algorithm is employed [32]. As we do not have the instability in optimization, any regulation scheme for topology optimization (the filtering scheme) is not necessary.

3.1. Sensitivity analysis example

The characteristics and accuracy of the sensitivity analysis of (13) are tested for the channel structure in Fig. 2. The rectangular fluid domain is set to the analysis domain (0.05 m by 0.03 m) discretized by 50 by 50 9-node elements (the 2nd order shape function for fluid velocity, the 1st order shape function for fluid pressure). Without the loss of generality, a silica particle with 4.78 μm for its diameter and 1900 kg/m^3 for its density is considered. The mass m_p and the drag force term F_D are computed accordingly. Due to the large ratio between the drag force and the mass, a very small time step is required to maintain the numerical stability. To test the accuracy of the sensitivity analysis with the different fluid velocity, the parabolic fluid with the maximum velocity, 0.0025 m/s or 0.25 m/s flows from the left side to the right outlet in Figs. 2 and 3. The following objective function $c(\mathbf{v})$ is considered as the objective function.

$$c(\mathbf{v}) = \int_0^{t_f} \|\mathbf{v}\|^2 \,\mathrm{dt} \tag{17}$$

Fig. 3 shows the comparisons with the sensitivity analysis and the finite difference method for several design variables and several simulation conditions. As shown, the very accurate computations can be possible. During the transient analysis for the movement of the silica particle, it is necessary to save all the velocities of the particle during the simulation time for the adjoint system. From a computational point of view, as only one particle is considered, the memory usage for saving the state of the particle is not a significant issue. In addition, the objective function being calculated by the time integration, it is possible to compute and save the pseudo force term $\frac{\partial c}{\partial \mathbf{v}}$ in Eq. (14) during the forward solution and the transient adjoint variable, $\boldsymbol{\lambda}$, can be analyzed with the saved pseudo

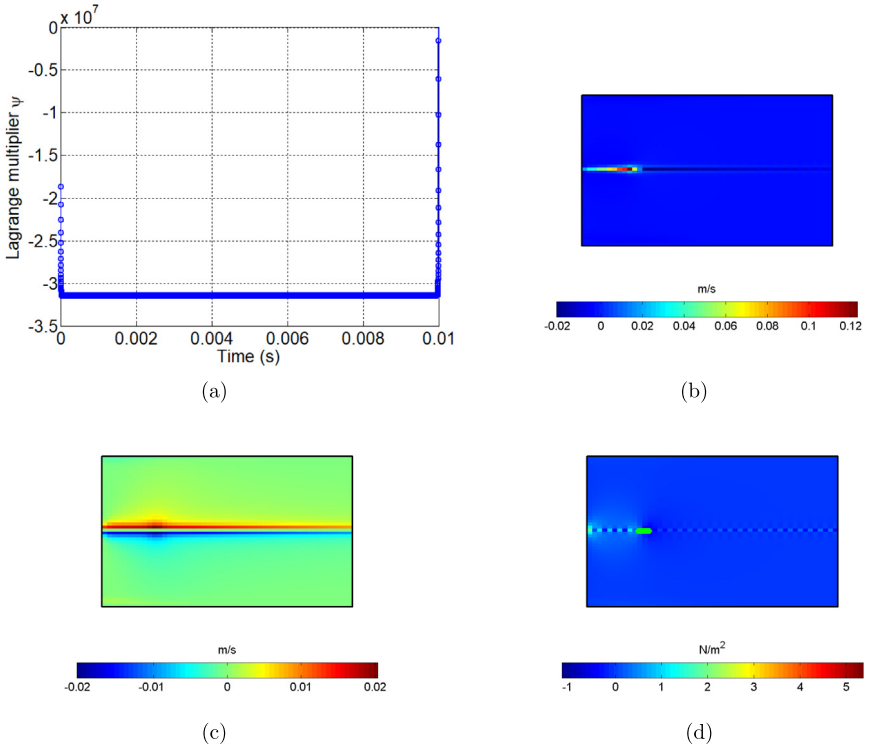

Fig. 6. Lagrange multipliers (Maximum velocity = 0.25 m/s, initial design = 0.5, simulation time t_f: 0.01 s, time step = 10,000 steps (Newmark scheme)). (a) The x component of the Lagrange multiplier $\boldsymbol{\lambda}$, (b, c, and d) the x-velocity, the y-velocity and the pressure of $\int_0^{t_f}(\boldsymbol{\psi})\mathrm{dt}$.

force term. The saved dimensions of the displacement, velocity, and acceleration of the particle are same as those of the adjoint variable, $\boldsymbol{\lambda}$. The second Lagrange multiplier variable $\boldsymbol{\psi}$ can be computed through equation (15). As stated before, the Lagrange multiplier variable $\boldsymbol{\psi}$ is also a transient variable. However, with the assumption of the steady state laminar flow, the integration of the Lagrange multiplier variable $\boldsymbol{\psi}$ can be employed for the final sensitivity analysis. For example, Figs. 4–6 show the Lagrange multipliers of the system with the different conditions. The first Lagrange multiplier of $\boldsymbol{\lambda}$ has zeros in the y-direction and non-zeros in the x-direction. The detail values can be found in Figs. 4–6.

3.2. Topology optimization example 1: Channel design problem 1

For the first optimization example, the topological optimization problem maximizing the integral of the fluid velocity over the analysis time subject to the mass constraint is solved for the structure in Fig. 2; the objective function is the integration of the square of the velocity of a particle and the mass constraint in fluid domain is imposed in (18). The design domain is discretized by 100 by 100 elements. By distributing the spatial materials at the fluid design domain and increasing the magnitude of fluid velocity, it aims to increase the norm of the velocities of the particle from the center line.

$$\begin{aligned} &\underset{\boldsymbol{\gamma}}{\text{Maximize}} \int_0^{t_f} \|\mathbf{v}\|^2 \,\mathrm{dt} = (\text{the integration of the velocity norm})^2 \\ &\text{Subject to mass} \leqslant \text{mass}_0 \\ &\quad \boldsymbol{\gamma} = [\gamma_1, \gamma_2, \ldots, \gamma_{N_e}], \quad \gamma_{\min} \leqslant \boldsymbol{\gamma} \leqslant 1, \quad \gamma_{\min} = 0.001 \end{aligned} \tag{18}$$

where the objective function is the integration of the square of the mass velocity over the simulation time t_f and the number of the design variables is denoted by N_e. First of all, the initial position of the mass particle is set to (1 cm, 1.5 cm) whose y coordinate is set to the center of the domain. To maximize the objective function,

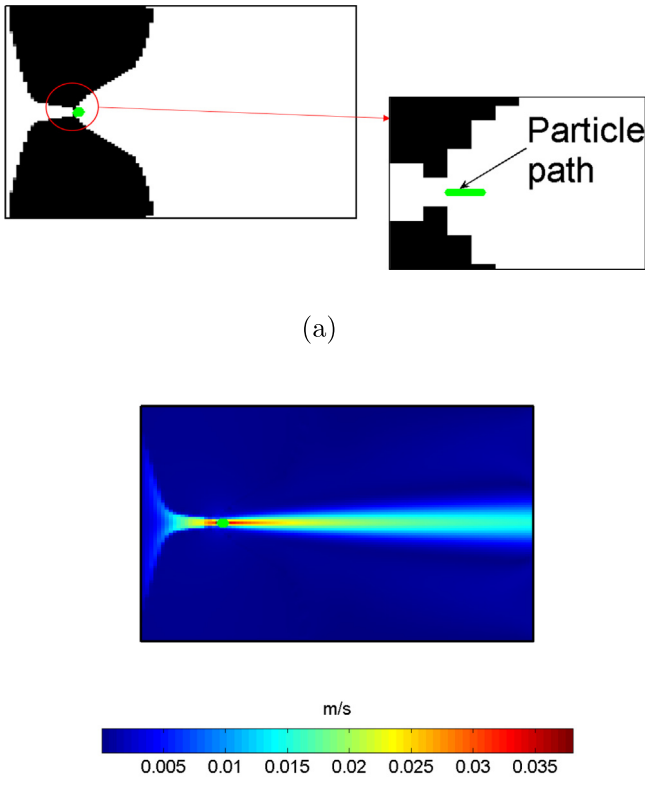

Fig. 7. Channel optimization example: (a) an optimized layout with 30% mass $t_f = 0.02$ s with 3000 time steps ($n = 3$, $\alpha_{max} = 10^5$, objective function: 2.8321×10^{-5} m^2/s) and (b) fluid velocity distribution.

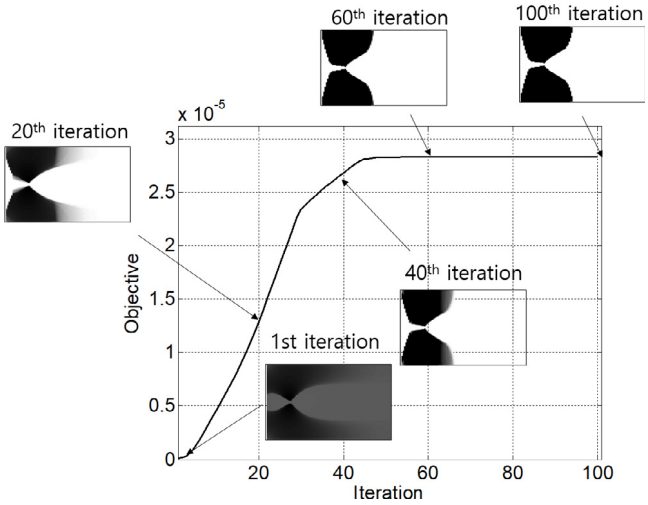

Fig. 8. The optimization convergence: the convergence of the objective function and the intermediate designs.

the optimal distributions of the large Darcy's force or the pseudo solid domain should be designed through the topology optimization process. It is expected that a channel configuration with a narrow orifice can be obtained as it maximizes the fluid velocity at the center line of the design domain. Fig. 7(a) shows an optimized layout

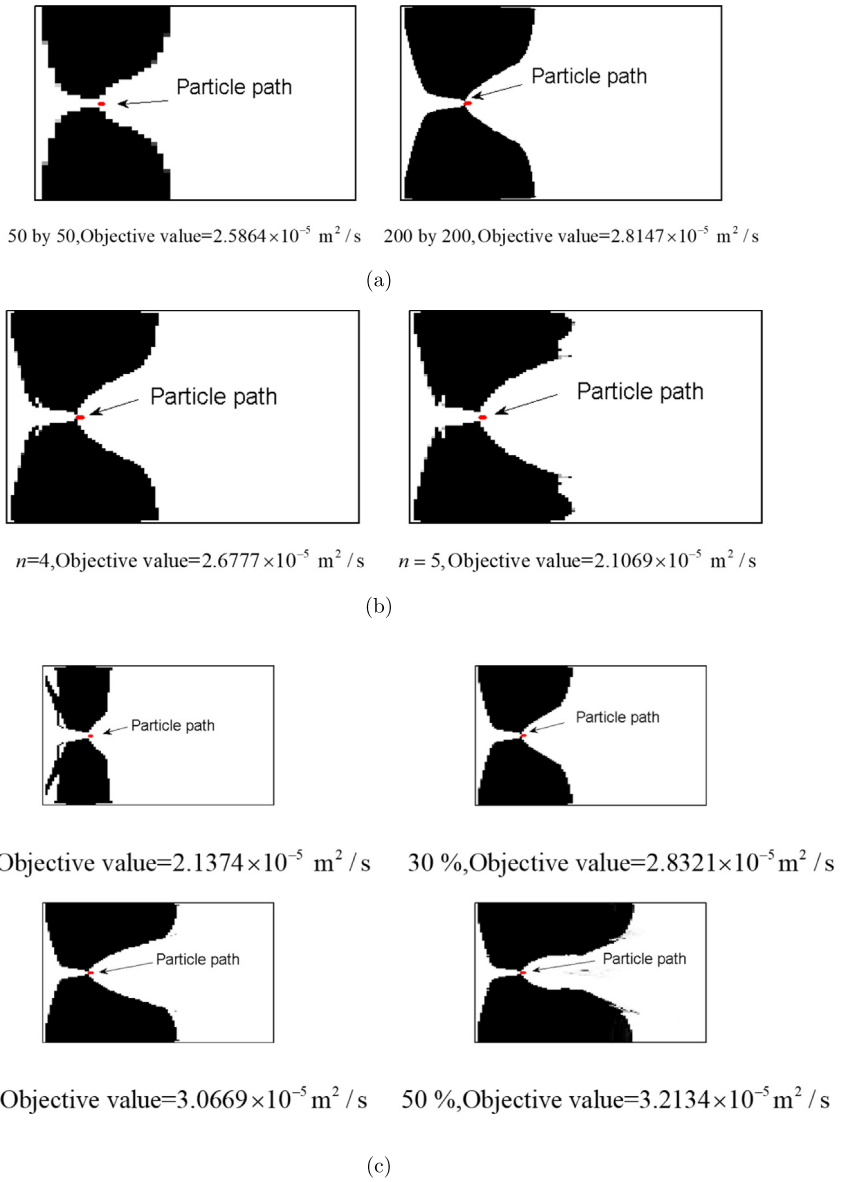

Fig. 9. Effect of mesh and penalization parameter. (a) Mesh effect, (b) the penalization effect and (c) the mass ratio test.

of the present optimization formulation with 0.02 s for the simulation time. As expected, the channel shape can be obtained in order to maximize the fluid velocity at the center line as shown in Fig. 7(b). The maximum fluid velocity can be increased up to 0.0380 m/s with the present optimization formulation. The convergence of the objective function and the intermediate optimal layouts are plotted in Fig. 8. As illustrated, the present optimization process can find out an optimized layout successfully and compared with the objective and the trajectory of the void design, the objective function is increased about 226 times (Objective value of the optimized layout: 2.8321 $\times 10^{-5}$ m^2/s, objective value of the void layout: 1.2508 $\times$ 10^{-7} m^2/s). The particle of the optimized layout can reach to 0.01075 m (displacement = 7.5235 $\times$ 10^{-4}m) in the x-direction where the particle of the void layout can only reach to 0.01005 m (displacement = 5.0002 $\times$ 10^{-5}m) in the x-direction. When minimizing (rather than maximizing) the objective function, a solid design appears near the initial position (1 cm, 1.5 cm) of the particle as the fluid velocity at the initial position converges zero and not to mention, no motion occurs. Fig. 9 shows the effects of the mesh refinement, the SIMP penalization effect and the mass ratio. The optimum designs with the

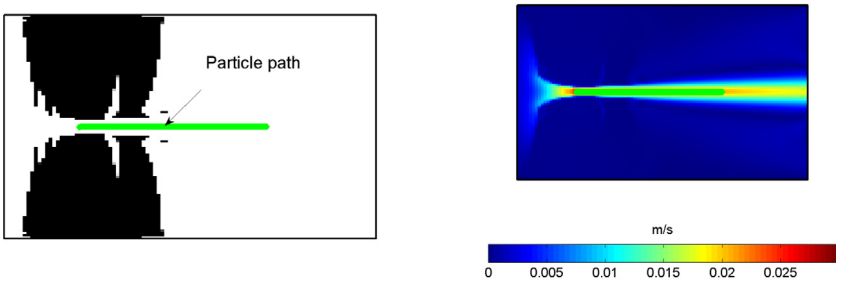

(a) (b)

Fig. 10. Channel optimization example: (a) an optimized layout with 30% mass, $t_f = 1$ s with 150,000 time steps (objective function: 6.5047×10^{-4} m^2/s) and (b) fluid velocity distribution.

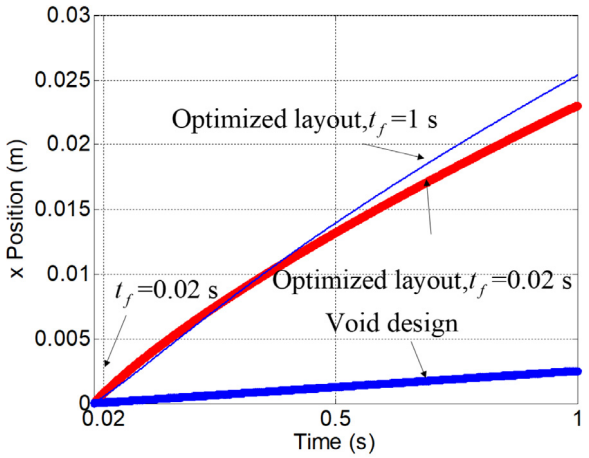

(a)

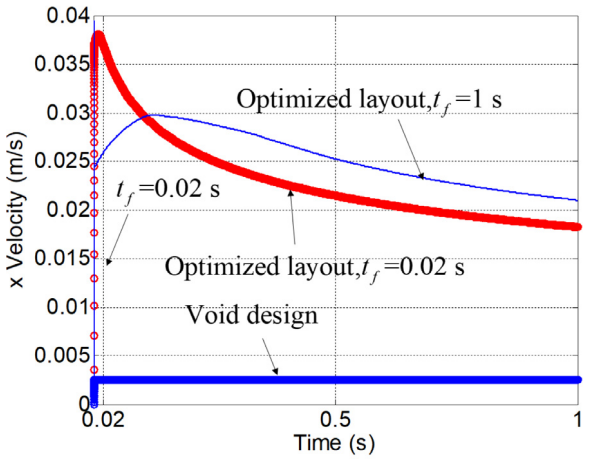

(b)

Fig. 11. Channel optimization example: (a and b) the position and the velocity comparisons with the optimized layouts and the void design.

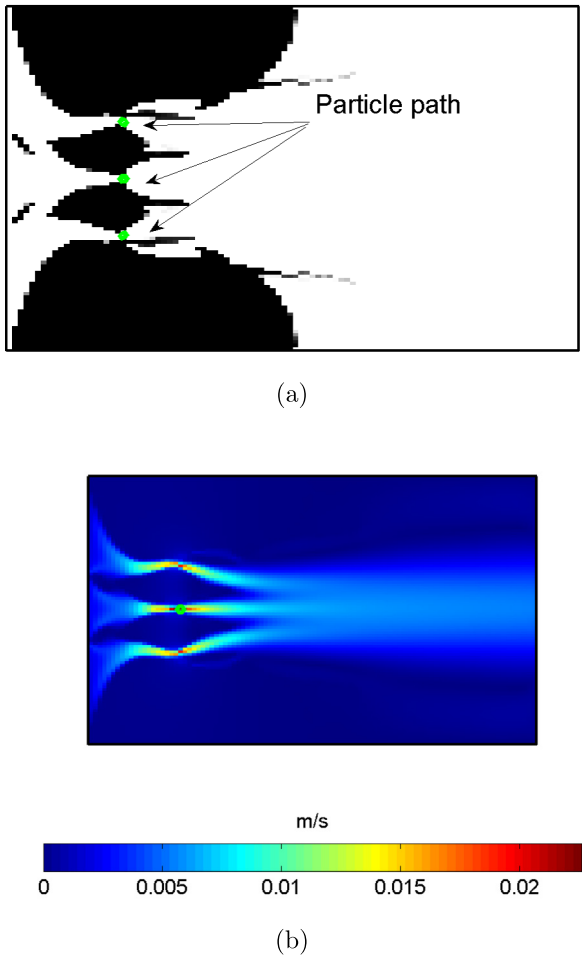

Fig. 12. Channel optimization example with three particles: (a) an optimized layout with 30% mass $t_f = 0.02$ s (objective function: 2.6434×10^{-5} m^2/s) and (b) fluid velocity distribution.

different mesh refinements are similar to each other with some differences in the objective functions due to the increase of the fluid velocity and the drag force. As observed in structural problem, the local optima are obtained depending on the value of the SIMP penalization. By increasing the mass ratio, the optimal layouts similar to the expansion chamber or the nozzle can be obtained in Fig. 9(c). In order to test the effect of the simulation time, t_f, Fig. 10 shows the optimized layout with $t_f = 1$ s with 150,000 time steps. The different layout can be obtained with 0.0353 m (displacement = 0.0253 m) in the x-direction for the final position. The sharp internal hole along the particle path can be observed. In order to test this feature further, the responses of the designs for 1 s, i.e., the designs in Figs. 7 and 10, are compared in Fig. 11. It turns out that the design in Fig. 7 is better from 0 s to 0.02 s in terms of the objective function or the integration of the velocity. The higher velocity can be obtained (red line) in Fig. 11(b) before 0.02 s and the velocity is decreased after that. However, the design optimized from 0 s to 1 s in Fig. 10 has a smaller velocity before 0.02 s compared with the design in Fig. 7 but it maintains the higher velocity for 1 s and it can move far as shown in Fig. 11(a). As an extension for multiple particles, Fig. 12 shows an optimal layout with three particles distributed along the y-direction. An optimal layout for multiple particles can be obtained through the present optimization method. Through these problems, it is shown that the present topology optimization framework can be an effective tool to design a channel considering the motion of particle.

For the sake of the test of the effect of the different initial location of the particle on the optimal layout, the initial location of the particle is changed for the optimized layouts in Figs. 13 and 14; the initial location of the mass is set to (1 cm, 0.5 cm) with (0.2 s, 30,000 steps). As expected, the optimized layout maximizing the fluid velocity

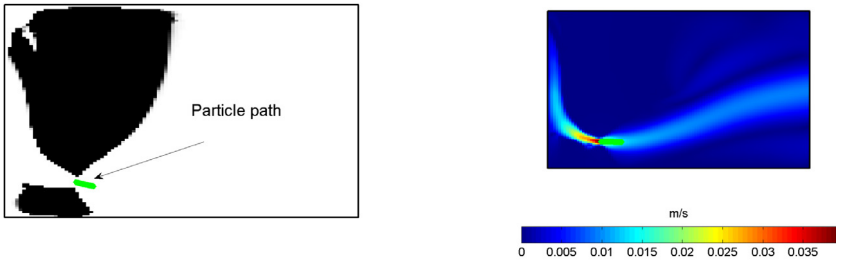

Fig. 13. An optimized channel with the particle at (1 cm, 0.5 cm) : (a) optimized design with 30% mass (objective function: 3.7081×10^{-5} m^2/s) and (b) velocity distribution.

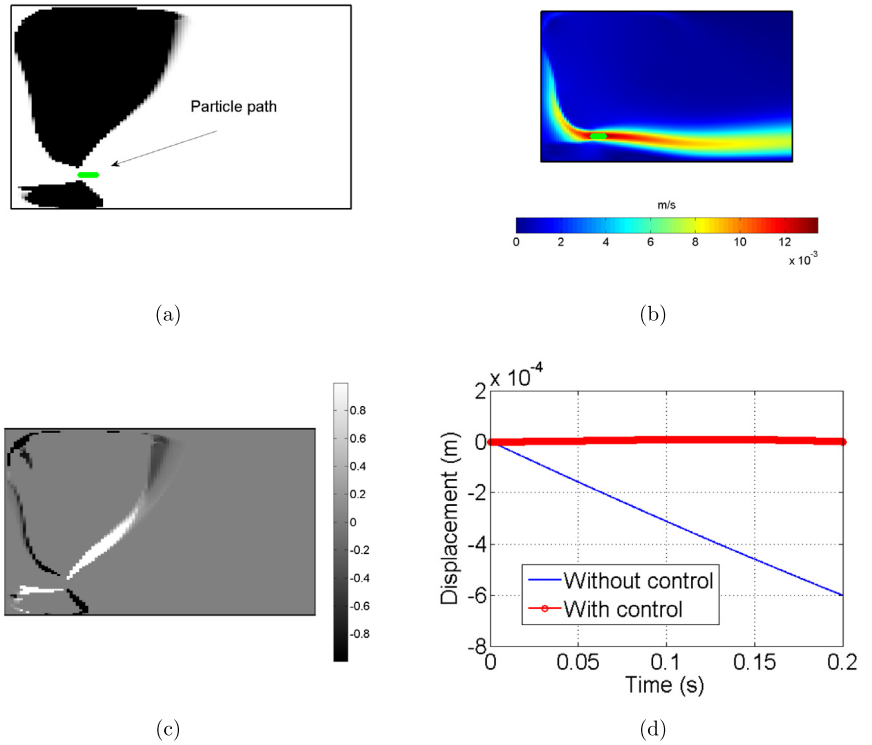

Fig. 14. Straight movement example: (a) an optimized design with 30% mass considering the optimization formulation in (19) (objective function: 3.5178×10^{-5} m^2/s) and (b) the velocity distribution, (c) the subtraction of the design variables ($\boldsymbol{\gamma}$ of Fig. 13(a) - $\boldsymbol{\gamma}$ of Fig. 14(a)), and (d) the comparison with the displacements in the y-direction. (For interpretation of the references to color in this figure legend, the reader is referred to the web version of this article.)

just before the initial location is obtained. Due to the unsymmetrical design in Fig. 13, the oblique trajectory or the curved trajectory of the particle following the fluid motion can be observed. While maximizing the velocity, the curve trajectory of the particle can be obtained. In order to find out a channel enabling the straight movement of particle, the following objective function maximizing the velocity in the x-direction and minimizing the velocity in the y-direction is considered in the optimization problem of (19). With the help of this optimization formulation, it is intended to obtain an optimal layout allowing a straight movement of the particle. To illustrate this feature, Fig. 14(a) shows an optimal layout with the initial position (1 cm, 0.5 m), where the original optimization formulation provides an optimal layout generating circular movement as shown in Fig. 14(d)(the blue line), the modified optimization formulation can provide an optimal channel allowing the relatively straight line. Fig. 14(c) shows the difference of

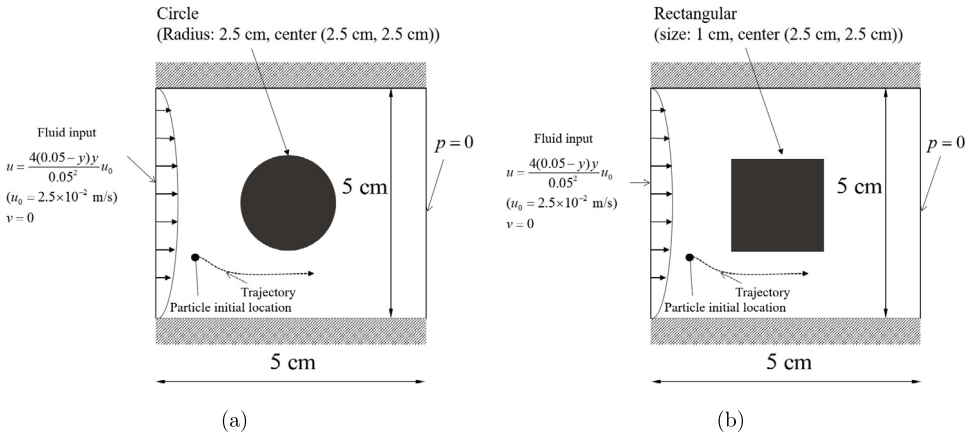

Fig. 15. Example 2. A channel design to maximize the particle velocity (Input velocity: 2.5×10^{-2} m/s, Reynolds number: 3551 ($1000 \times 0.05 \times 2.5 \times 10^{-2}/352 \times 10^{-6}$), Fluid: density = 1000 kg/m^3, viscosity = 352×10^{-6} Pa×s, Particle: mass = 1.0865 $\times 10^{-13}$ kg, $F_D = 1.5857 \times 10^{-8} \frac{\text{N·s}}{\text{kg·m}}$, mass$_0$: 20 % of the design domain).

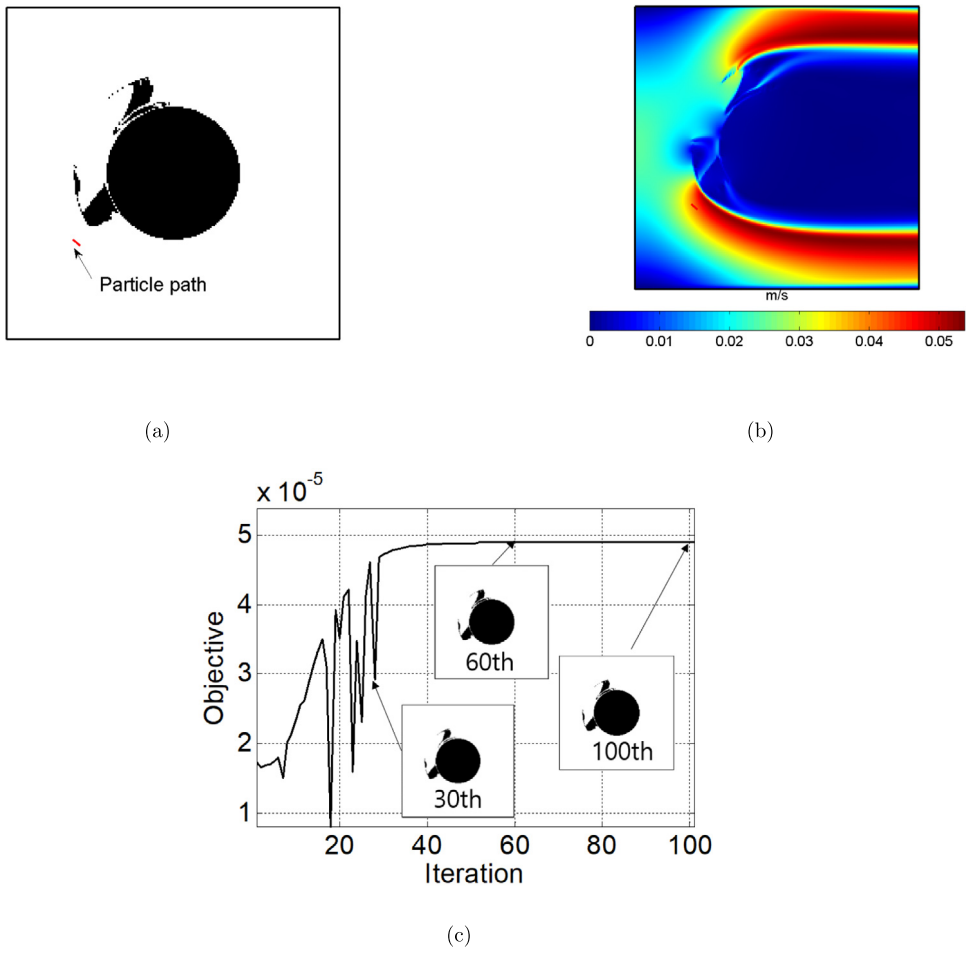

Fig. 16. Optimization result with the solid circular structure: (a) an optimized design with 20% mass (objective function: 4.9023×10^{-5} m^2/s), (b) its velocity distribution, and (c) the optimization history.

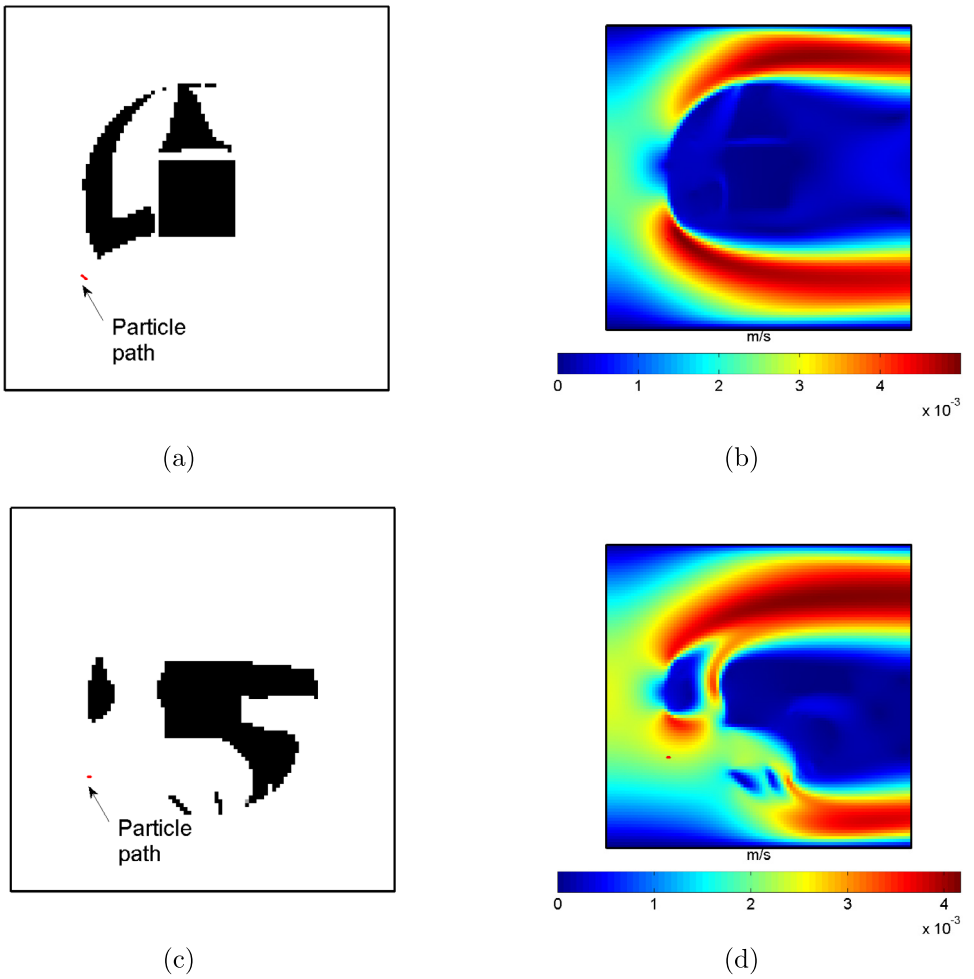

Fig. 17. Optimization results with the solid rectangular structure: (a and b) an optimized design with 20% mass and its velocity distribution without the control (Simulation time (t_f): 0.18 s, objective function: 3.1558×10^{-6} m^2/s) and (c and d) an optimized design with 20% mass and its velocity distribution with the control (Simulation time (t_f): 0.18 s, objective function: 8.4618×10^{-7} m^2/s).

the density distributions of Figs. 13(a) and 14(a). It shows that the outer perimeters are changed in order to have the straight motion in Fig. 14(d). In other words, it is found that the front of the upper part of the design in Fig. 13(a) moves back and the front part of the lower part of the design in Fig. 13(a) moves front in order to make the fluid motion straight around the slit. In the rear parts, the opposite phenomenon occurs.

$$\begin{aligned} &\underset{\boldsymbol{\gamma}}{\text{Max}} \int_0^{t_f} \|\mathbf{v}_x\|^2 - \|\mathbf{v}_y\|^2 \mathrm{dt} \\ &\text{Subject to mass } \leqslant \text{mass}_0 \\ &\boldsymbol{\gamma} = [\gamma_1, \gamma_2, \ldots, \gamma_{N_e}], \quad \gamma_{\min} \leqslant \boldsymbol{\gamma} \leqslant 1 \end{aligned} \tag{19}$$

where the velocities in the x direction and the y direction are denoted by $\mathbf{v}_x$ and $\mathbf{v}_x$, respectively.

3.3. Topology optimization example 2: Channel design problem with resistant solid circular and rectangular structures

For the second optimization example, the optimization problems shown in Fig. 15 are considered; the material properties and the dimension are similarly set as those of the first example. In this example, the input fluid flows

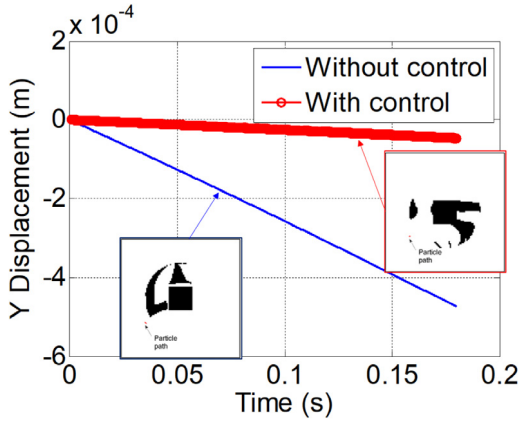

(a)

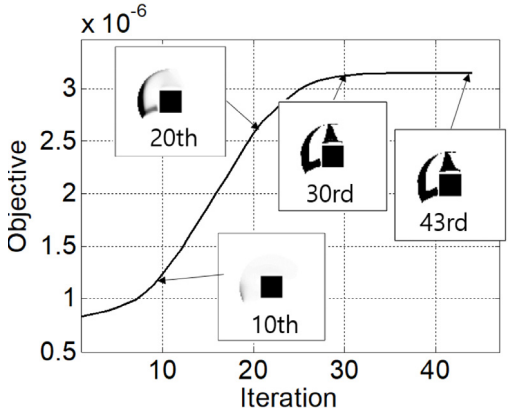

(b)

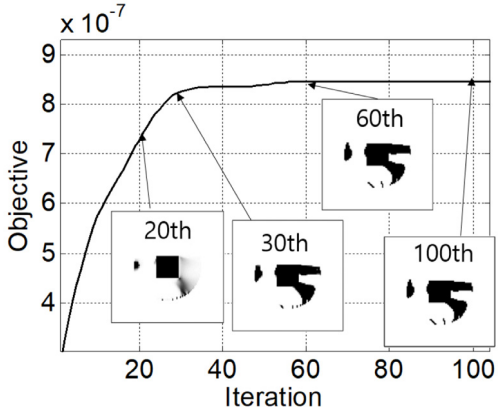

(c)

Fig. 18. Comparison of the displacements in the y-direction of the designs in Fig. 17 and the optimization histories.

around the circular solid or the rectangular solid. Indeed, the particle whose initial location is (1 cm, 1.5 cm) follows the streamlines around the solid structures. The objective of this optimization problem is also set to maximize the fluid velocity subject to the 20% mass constraint.

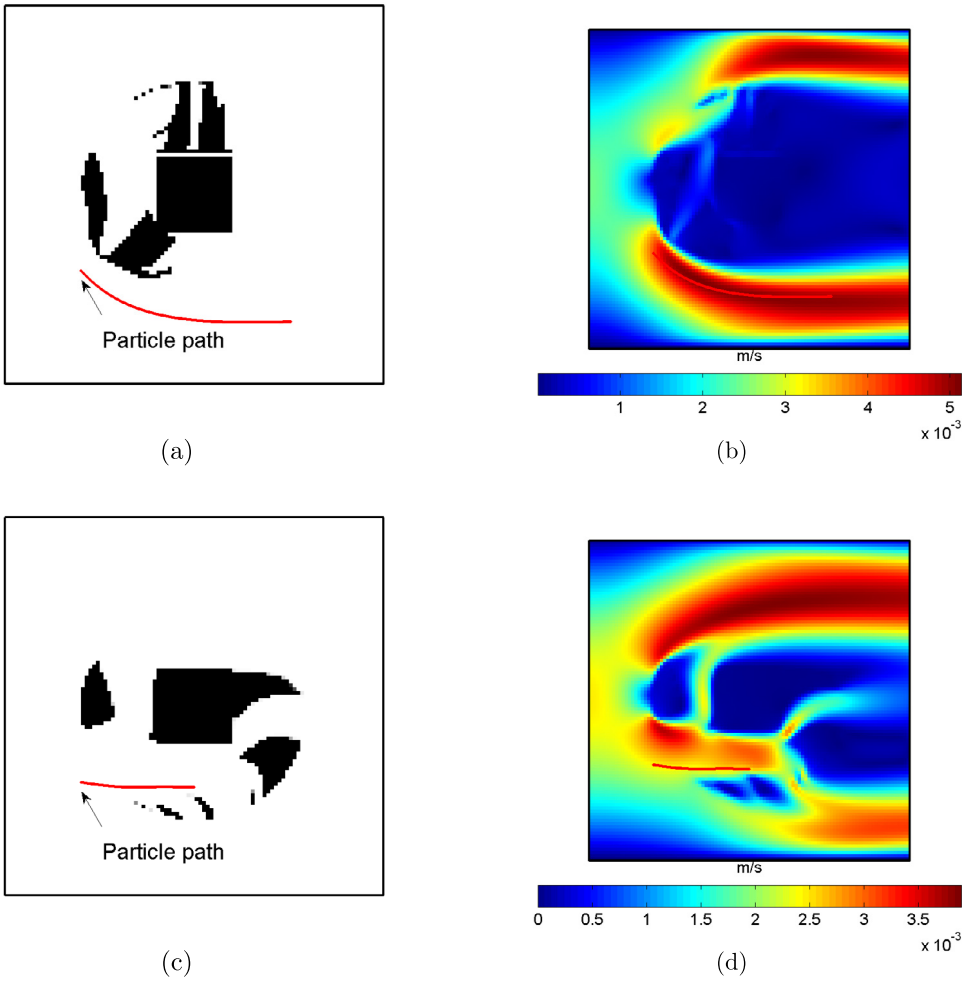

Fig. 19. Optimization results with the solid rectangular structure: (a and b) an optimized design with 20% mass and its velocity distribution without the control (Simulation time (t_f): 6 s, objective function: 1.4613×10^{-4} m^2/s) and (c and d) an optimized design with 20% mass and its velocity distribution with the control (Simulation time (t_f): 6 s, objective function: 2.7284×10^{-5} m^2/s).

Fig. 16 shows an optimal layout for 0.03 s with 15,000 time steps with the solid circular structure. The two large trapezoid structures appear first and the small structures appear in order to guide the fluid underneath the circle. For another test, the solid rectangular is placed at the center for the optimized layout in Fig. 17 for 0.18 s. In these two configurations, it is possible to obtain the optimized layouts to maximize the fluid velocity around the resistant structures. Note that the optimized structures are difficult to image by engineer. To make the trajectory of the particle straight, the optimization formulation in (19) is also solved for the optimized layout in Fig. 17(c) and (d). As shown in Fig. 17(d), the complex fluid motion can be obtained in order to have the straight motion of the particle. The comparison of their responses and the iteration histories are given in Fig. 18. With the two optimized designs, the curved trajectories of the particle are obtained. Figs. 19 and 20 show the optimal designs with and without the controlling of the vertical motion and their responses for 6 s. By increasing the simulation time, the particle can travel further and the different designs can be obtained. In order to make the particle travel further, a slit at the rear part is introduced in Fig. 18. Fig. 19(c) allowing the fluid flow out to the upper domain. Due to the control, the particle in Fig. 19(c) moves slower than the particle in Fig. 19(a). Fig. 20 shows the responses and the optimization histories of the designs. This example also illustrates that the present sensitivity analysis and the optimization formulation work properly in connection with the particle and the fluid coupling analysis.

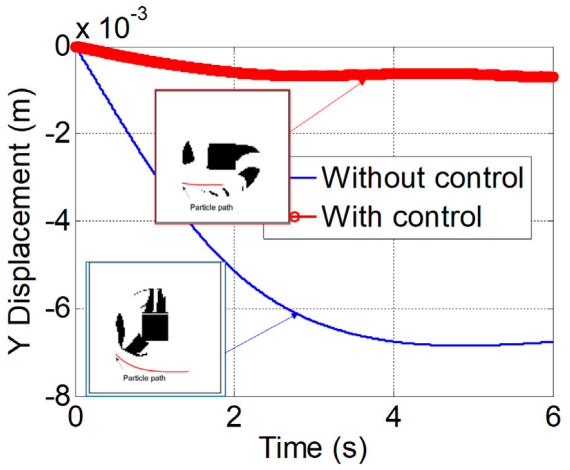

(a)

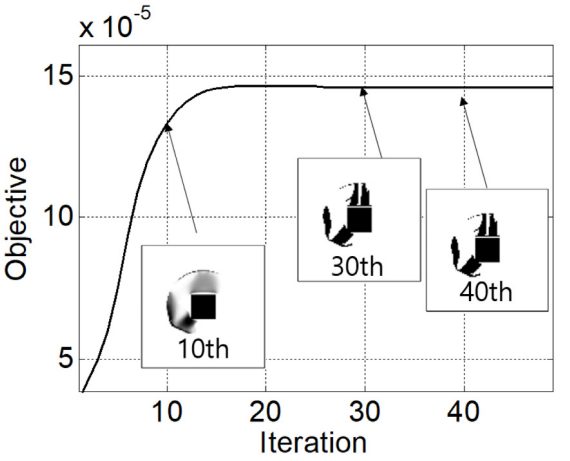

(b)

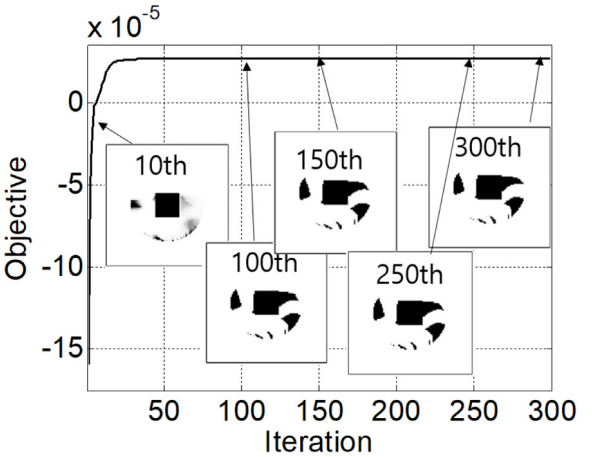

(c)

Fig. 20. Comparison of the displacements in the y-direction of the designs in Fig. 19 and the optimization histories.

4. Conclusions

This research focus on a new topology optimization method for optimal layouts considering the transient motion of particle in fluid. It is an important engineering problem to consider the motion of particle in fluid. For this, this research derives a new transient sensitivity analysis which can be extended to transient flow and develops a new topology optimization formulation considering the velocity profile of particle in fluid. The steady state laminar fluid is assumed and the effect of particle on fluid is neglected. The adjoint sensitivity analysis for the multiphysics system requires the two time varying Lagrange multipliers. Although the steady state laminar fluid is assumed, the time varying Lagrange multipliers for the steady state Navier–Stokes equation are necessary. This is due to that the force terms of the adjoint equation originated from the Newton's 2nd law of particle are the time varying forces. The integration of the velocities of particle is considered for the objective function with the mass constraint. In order to show the validity of the present formulations, several optimization problems are considered. The optimal layouts controlling the particle motion and the fluid motion can be obtained. For future research, the optimization of the motions of several particles considering the contact among particles and wall should be considered in order to examine local particle concentration, migration and segregation. This work is just one example of these general scientific and engineering frameworks applied to the particle in fluid. In addition, the mixing of particles in 3 dimensional turbulent flow also can be researched. We should check how far the particle modeling can be realized. In addition, to consider transient flow, a new sensitivity analysis also should be formulated.

Declaration of competing interest

The authors declare that they have no known competing financial interests or personal relationships that could have appeared to influence the work reported in this paper.

Acknowledgment

This work was supported by the National Research Foundation of Korea (NRF) grant funded by the Korea government (MSIT) (NRF-2019R1A2C2084974).

References

[1] X.L. Qiu, J.H. Huang, T.M. Westerhof, J.A. Lombardo, K.M. Henrikson, M. Pennell, P.P. Pourfard, E.L. Nelson, P. Nath, J.B. Haun, Microfluidic channel optimization to improve hydrodynamic dissociation of cell aggregates and tissue, Sci. Rep. 8 (2018) 2774.
[2] X.L. Qiu, J. De Jesus, M. Pennell, M. Troiani, J.B. Haun, Microfluidic device for mechanical dissociation of cancer cell aggregates into single cells, Lab Chip 15 (1) (2015) 339–350.
[3] J.J. Wylie, D.L. Koch, Particle clustering due to hydrodynamic interactions, Phys. Fluids 12 (5) (2000) 964–970.
[4] G.B. Mo, A.S. Sangani, A method for computing Stokes-flow interactions among spherical objects and its application to suspensions of drops and porous particles, Phys. Fluids 6 (5) (1994) 1637–1652.
[5] H. Lee, S. Balachandar, Drag and lift forces on a spherical particle moving on a wall in a shear flow at finite re, J. Fluid Mech. 657 (2010) 89–125.
[6] A. Dinler, I. Okumus, Inertial particle separation in curved networks: A numerical study, Chem. Eng. Sci. 182 (2018) 119–131.
[7] Y.-C. Wu, B. Yang, An overview of numerical methods for incompressible viscous flow with moving particles, Arch. Comput. Methods Eng. 26 (4) (2019) 1255–1282.
[8] D. Makhija, G. Pingen, R. Yang, K. Maute, Topology optimization of multi-component flows using a multi-relaxation time lattice Boltzmann method, Comput. & Fluids 67 (2012) 104–114.
[9] M.P. Bendse, N. Kikuchi, Generating optimal topologies in structural design using a homogenization method, Comput. Methods Appl. Mech. Engrg. 71 (2) (1988) 197–224.
[10] M.Y. Wang, X. Wang, D. Guo, A level set method for structural topology optimization, Comput. Methods Appl. Mech. Engrg. 192 (1) (2003) 227–246.
[11] W. Zhang, D. Li, J. Zhou, Z. Du, B. Li, X. Guo, A moving morphable void (MMV)-based explicit approach for topology optimization considering stress constraints, Comput. Methods Appl. Mech. Engrg. 334 (2018) 381–413.
[12] K. Maute, G.W. Reich, Integrated multidisciplinary topology optimization approach to adaptive wing design, J. Aircr. 43 (1) (2006) 253–263.
[13] A. Evgrafov, G. Pingen, K. Maute, Topology optimization of fluid domains: Kinetic theory approach, J. Appl. Math. Mech. Z. Angew. Math. Mech. 88 (2008) 129–141.
[14] E.M. Papoutsis-Kiachagias, K.C. Giannakoglou, Continuous adjoint methods for turbulent flows, applied to shape and topology optimization: Industrial applications, Arch. Comput. Methods Eng. 23 (2) (2016) 255–299.
[15] G.H. Yoon, Topological layout design of electro-fluid-thermal-compliant actuator, Comput. Methods Appl. Mech. Engrg. 209–212 (2012) 28–44.

[16] E.M. Dede, J. Lee, T. Nomura, Multiphysics Simulation: Electromechanical System Applications and Optimization, Springer-Verlag London, 2014.
[17] G.H. Yoon, Stress-based topology optimization method for steady-state fluid–structure interaction problems, Comput. Methods Appl. Mech. Engrg. 278 (2014) 499–523.
[18] K. Yaji, T. Yamada, M. Yoshino, T. Matsumoto, K. Izui, S. Nishiwaki, Topology optimization in thermal-fluid flow using the lattice Boltzmann method, J. Comput. Phys. 307 (2016) 355–377.
[19] Y. Deng, Z. Liu, P. Zhang, Y. Liu, Y. Wu, Topology optimization of unsteady incompressible Navier–Stokes flows, J. Comput. Phys. 230 (17) (2011) 6688–6708.
[20] G.H. Yoon, Topology optimization for turbulent flow with Spalart–Allmaras model, Comput. Methods Appl. Mech. Engrg. 303 (2016) 288–311.
[21] G.H. Yoon, Topological design of heat dissipating structure with forced convective heat transfer, J. Mech. Sci. Technol. 24 (6) (2010) 1225–1233.
[22] T. Dbouk, A review about the engineering design of optimal heat transfer systems using topology optimization, Appl. Therm. Eng. 112 (2017) 841–854.
[23] H.S. Damiri, H.K. Bardaweel, Numerical design and optimization of hydraulic resistance and wall shear stress inside pressure-driven microfluidic networks, Lab Chip 15 (21) (2015) 4187–4196.
[24] C. Prohm, F. Troltzsch, H. Stark, Optimal control of particle separation in inertial microfluidics, Eur. Phys. J. E 36 (10) (2013) 36–118.
[25] G. Pagano, M. Ventre, M. Iannone, F. Greco, P.L. Maffettone, P.A. Netti, Optimizing design and fabrication of microfluidic devices for cell cultures: An effective approach to control cell microenvironment in three dimensions, Biomicrofluidics 8 (4) (2014) 046503.
[26] H. Bockelmann, V. Heuveline, D.P.J. Barz, Optimization of an electrokinetic mixer for microfluidic applications, Biomicrofluidics 6 (2) (2012) 024123.
[27] H.H. Hu, D.D. Joseph, M.J. Crochet, Direct simulation of fluid particle motions, Theor. Comput. Fluid Dyn. 3 (1992) 285–306.
[28] X.Y. Chen, Topology optimization of microfluidics - A review, Microchem. J. 127 (2016) 52–61.
[29] M.J. Walsh, Influence of Particle Drag Coefficient on Particle Motion in High-Speed Flow with Typical Laser Velocimeter Applications, Report, NASA, 1976.
[30] P.M. Kulkarni, J.F. Morris, Pair-sphere trajectories in finite-reynolds-number shear flow, J. Fluid Mech. 596 (2008) 413–435, http://dx.doi.org/10.1017/S0022112007009627.
[31] G. Bagheri, C. Bonadonna, On the drag of freely falling non-spherical particles, Powder Technol. 301 (2016) 526–544.
[32] K. Svanberg, The method of moving asymptotes – a new method for structural optimization, Internat. J. Numer. Methods Engrg. 24 (2) (1987) 359–373.